Colossal electroresistance mechanism in a $Au/Pr_{0.7}Ca_{0.3}MnO_3/Pt$ sandwich structure: Evidence for a Mott transition

D. S. Kim,[1,2] Y. H. Kim,[1,*] C. E. Lee,[2] and Y. T. Kim[1]
[1]*Semiconductor Devices Laboratory, Korea Institute of Science and Technology, Seoul 136-791, Korea*
[2]*Department of Physics, Korea University, Seoul 136-701, Korea*
(Received 9 May 2006; revised manuscript received 13 September 2006; published 28 November 2006)

The resistive switching characteristics of $Au/Pr_{0.7}Ca_{0.3}MnO_3$(PCMO)/Pt sandwich structure were investigated by changing growth temperature of the PCMO film, adding an oxygen annealing process, and modifying the Au/PCMO/Pt sandwich structure by inserting a $PrMnO_3$ (PMO) or $CaMnO_3$ (CMO) layer at the Au/PCMO interface. From these experiments, we obtained the following results. First, only crystalline PCMO films exhibited reversible resistive switching behavior in Au/PCMO/Pt sandwich structure. Secondly, the Mn^{4+}/Mn^{3+} ratio at the PCMO surface was changed by oxygen annealing of the PCMO film, resulting in an increase of the resistance ratio of high resistance state and low resistance state. Lastly, we could not observe the resistive switching behavior in Au/PMO/PCMO/Pt and Au/CMO/PCMO/Pt sandwich structures. The resistive switching behavior could be observed only in Au/PCMO/PMO(or CMO)/PCMO/Pt sandwich structure. These results indicate that the resistive switching of Au/PCMO/Pt sandwich structure depends on the mixed valence state Mn^{4+}/Mn^{3+} of Mn ions in the metal/PCMO interface domains. This result can be regarded as evidence for a Mott transition.

DOI: 10.1103/PhysRevB.74.174430 PACS number(s): 75.47.Lx, 73.40.−c, 85.30.De, 81.15.Fg

I. INTRODUCTION

$Pr_{1-x}Ca_xMnO_3$ has attracted considerable interest due to its unusual magnetic and electronic properties, such as colossal magnetoresistance (CMR) (Refs. 1–6) and colossal electroresistance (CER).[7–17] Among these properties, CER has recently been explored in detail because of its potential for device applications such as nonvolatile resistance random access memories, since Liu *et al.* reported that reversible resistance change can be induced by applying pulsed voltage to the $Pr_{0.7}Ca_{0.3}MnO_3$ (PCMO) layer sandwiched between a Ag top-electrode and a $YBa_2Cu_3O_7$ or Pt bottom electrode at room temperature.[7] However, the origin of CER at room temperature is yet to be elucidated.[10–12] The ground state of $Pr_{1-x}Ca_xMnO_3$ with $x=0.3-0.5$ is known to be a charge-ordered antiferromagnetic insulator, which can be switched to a ferromagnetic metal by applying strong magnetic or electric fields.[8–10] However, at room temperature, $Pr_{1-x}Ca_xMnO_3$ is not close to any phase boundary between competing phases and is in a paramagnetic insulating state regardless of x.[6] Therefore, the origin of CER at room temperature is difficult to explain, and thus it is important to elucidate the mechanism of the resistive switching of PCMO films. In this work, we thus studied CER mechanism of the Au/PCMO/Pt sandwich structure by changing the growth temperature of the PCMO films, adding the oxygen annealing process after deposition, and modifying the Au/PCMO/Pt structure by introducing $PrMnO_3$ (PMO) or $CaMnO_3$ (CMO) layer into the structure in order to find out some experimental clues for elucidating the origin of CER mechanism of the Au/PCMO/Pt structure.

II. EXPERIMENTS

To investigate the resistive switching characteristics of the Au/PCMO/Pt sandwich structures, the PCMO films were grown on $Pt/Ti/SiO_2/Si(100)$ substrates by using pulsed laser deposition (PLD) employing a KrF excimer laser with a wavelength of 248 nm. The target was synthesized by using a conventional solid-state reaction and its composition was $Pr_{0.7}Ca_{0.3}MnO_3$. The PCMO films were deposited at the substrate temperature (T_s) ranging from 500 to 700 °C under oxygen pressure of 300 mTorr with constant laser energy density of 2 J/cm^2 and constant laser repetition rate of 5 Hz. The distance between target and substrate was fixed to 5 cm. Au top electrodes with a diameter of ~200 μm were deposited on the PCMO films by thermal evaporation under a base pressure of $<5\times10^{-6}$ Torr with a dot-patterned metal shadow mask.

The oxygen-annealing effect on the resistive switching phenomenon of the PCMO film was investigated. For this, the PCMO films were deposited at $T_s=700$ °C under oxygen pressure of 200 mTorr. After deposition, the films were *in situ* annealed at 500 °C for 1 h under oxygen pressure of ~200 Torr.

The Au/PCMO/Pt sandwich structure was modified by inserting PMO or CMO layer into the sandwich structure. Two types of the sandwich structure were prepared as follows: (i) Au/PMO(or CMO)/PCMO/Pt and (ii) Au/PCMO/PMO(or CMO)/PCMO/Pt. These structures were *in situ* fabricated by PLD at the substrate temperature of 700 °C under oxygen pressure of 300 mTorr. The other deposition conditions were the same as those for the PCMO films as described above. In structure (i), the thickness of the PCMO film was ~360 nm and that of the PMO (or CMO) layer was varied from 5 to 30 nm. In structure (ii), the thickness of the PCMO film was ~30 nm and that of the PMO (or CMO) layer was ~360 nm. In addition, Au/PMO(or CMO)/Pt structure was fabricated using the same deposition conditions by PLD for investigating the characteristic of the PMO (or CMO) layer itself.

The crystal structures of the PCMO film and the multilayered films were investigated by x-ray diffraction (XRD).

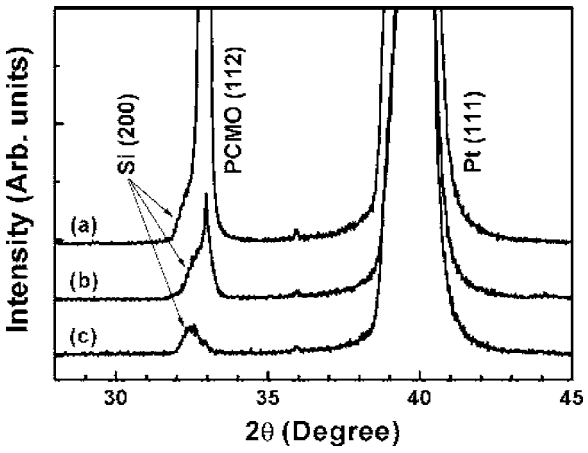

FIG. 1. XRD patterns of PCMO thin films deposited on $Pt/Ti/SiO_2/Si(100)$ substrates at various substrate temperatures of (a) T_s=700 °C, (b) T_s=600 °C, and (c) T_s=500 °C.

The chemical composition of oxygen-annealed and as-grown PCMO films were analyzed by x-ray photoelectron spectroscopy (XPS) using a PHI 5800 ESCA system. Current-voltage (I-V) characteristics of the sandwich structures were measured by using semiconductor parameter analyzer (Agilent 4155B). The voltage bias was scanned as $0 \rightarrow +V_{max} \rightarrow 0 \rightarrow -V_{max} \rightarrow 0$ V. Here, the positive bias was defined as the current flowing from the Pt bottom electrode to the Au top electrode. All measurements were performed at room temperature.

III. RESULTS AND DISCUSSION

Figure 1 shows XRD patterns of the PCMO thin films grown on $Pt/Ti/SiO_2/Si(100)$ substrates at various substrate temperatures under oxygen pressure of 300 mTorr. From this figure, the PCMO films were found to be crystallized at the substrate temperature of $\geqslant$600 °C and also only (112) peak of the PCMO film was found to exist, indicating that the PCMO films were grown with a (112)-preferred orientation on $Pt/Ti/SiO_2/Si(100)$ substrates. The crystallinity of the PCMO films was enhanced with increasing the substrate temperature.

Figure 2 shows the I-V characteristics of Au/PCMO/Pt sandwich structures in which the PCMO films were deposited at the substrate temperature of 500–700 °C under oxygen pressure of 300 mTorr. The voltage bias was scanned as $0 \rightarrow +0.8\ V \rightarrow 0 \rightarrow -0.8\ V \rightarrow 0$ V. Only crystalline PCMO films grown at $T_s \geqslant 600$ °C exhibited the hysteretic I-V characteristics. The resistive switching occurred from the high-resistance state (HRS) to low-resistance state (LRS) in a positive bias region and vice versa in a negative bias region. The resistance ratio of HRS and LRS increased with increasing the substrate temperature. The values of the resistance ratio measured at the bias voltage of +0.1 V are ~2.5 and ~14.5 for the PCMO films grown at 600 and 700 °C, respectively. This result implies that the resistive switching behavior of the PCMO film may be strongly related to the film crystallinity.

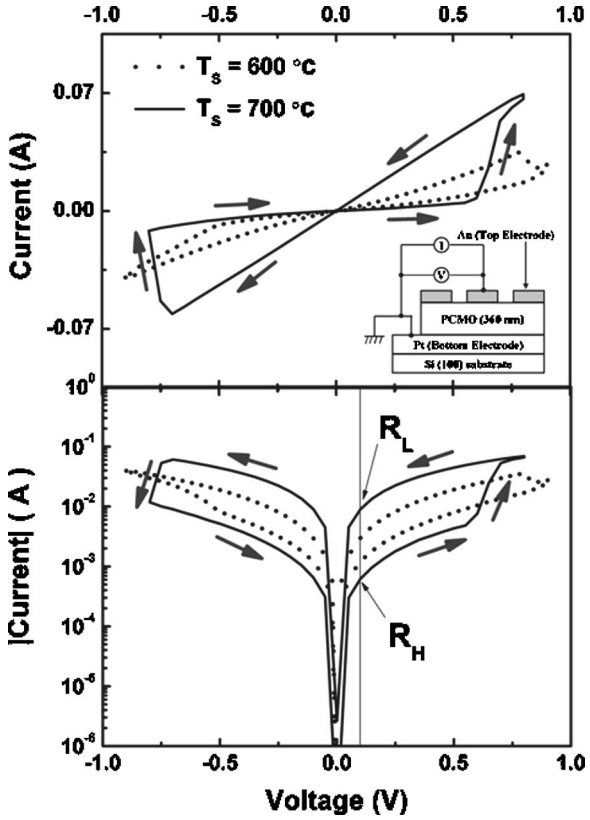

FIG. 2. I-V characteristics of Au/PCMO/Pt structures in which the PCMO films were deposited at various substrate temperatures. Arrows indicate the direction of the sweep. Top panel is drawn in linear scale. The inset panel shows schematic view of I-V measurement system. Bottom panel is drawn in semilogarithmic scale.

Figure 3 shows XRD patterns of as-grown and oxygen-annealed PCMO films. This figure shows that the as-grown PCMO film and the oxygen-annealed film have a little difference in the film orientation. The as-grown PCMO film exhibited (112) and (021) peaks, while the oxygen-annealed one shows only (112) peak. These results indicate that the film orientation of the PCMO film could be changed a little by oxygen annealing. In connection with our result, it was

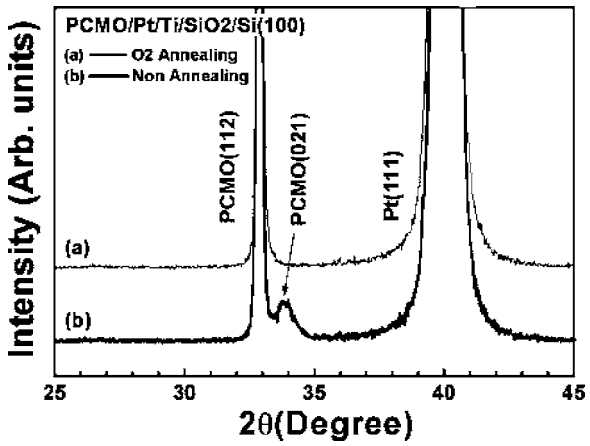

FIG. 3. XRD patterns of (a) oxygen-annealed PCMO film and (b) as-grown one deposited on $Pt/Ti/SiO_2/Si(100)$ substrates.

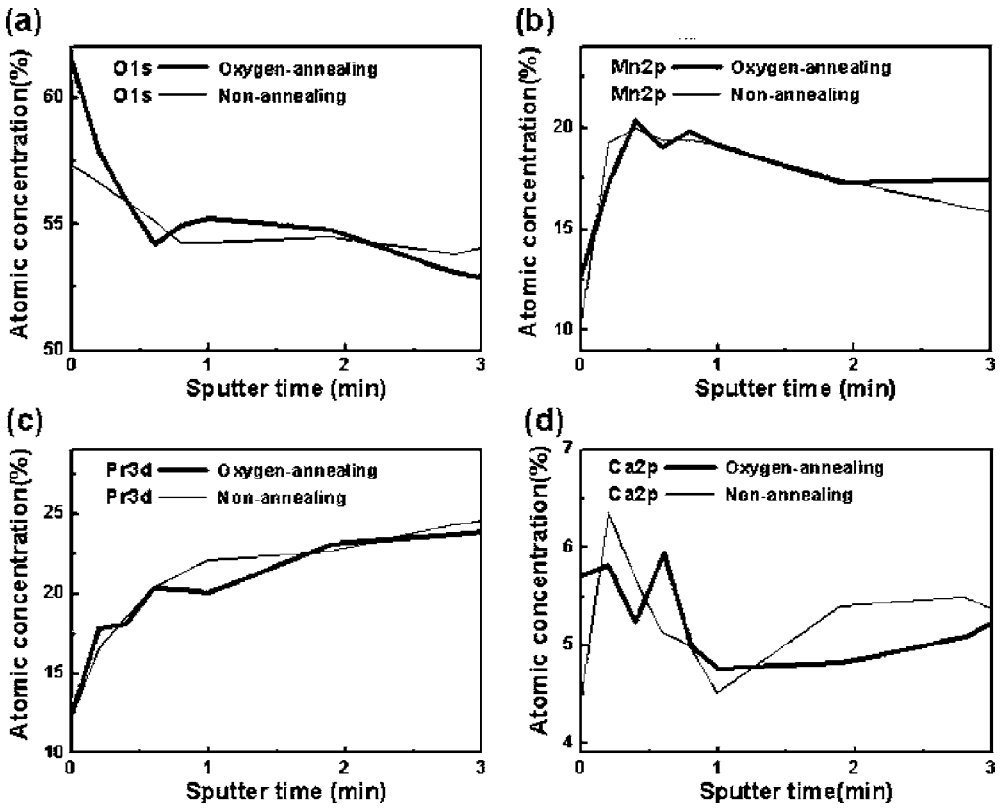

FIG. 4. Depth profiles of atomic concentrations of (a) oxygen, (b) manganese, (c) praseodymium, and (d) calcium of the oxygen-annealed PCMO film (plotted in thick line) and as-grown one (plotted in thin line).

reported that oxygen annealing of $La_{0.75}Ca_{0.25}MnO_3$ thin films resulted in its structural changes.[18]

Figure 4 shows the depth profiles of atomic concentrations of oxygen, manganese, praseodymium, and calcium for as-grown PCMO film (plotted in thin line) and oxygen-annealed film (plotted in thick line) measured by XPS. The etching rate of the PCMO film was ~120 Å/min by sputtering. From this figure, it was found that the oxygen-annealed PCMO film had a larger atomic concentration of oxygen than the as-grown one at a clean (original) PCMO surface. That is, as-grown and oxygen-annealed PCMO films had different oxygen stoichiometry at the film surface. This can be explained as follows. Under oxygen annealing the oxygen content in the film is increasing and we expect

$$\mathrm{Pr}_{1-x}\mathrm{Ca}_x\mathrm{MnO}_3 + (\delta/2)\mathrm{O}_2 \rightarrow \mathrm{Pr}_{1-x}\mathrm{Ca}_x\mathrm{MnO}_{3+\delta} = (\mathrm{Pr}_{1-x}\mathrm{Ca}_x)_{1-y}\square_y\mathrm{Mn}_{1-z}\square_z\mathrm{O}_3,$$

where □ represents cation vacancies and δ represents an excess of oxygen. Thus, excess oxygen leads to an equal number of vacancies at both of the cation sites and therefore to an increase of the Mn^{4+} content.[18,19] Consequently, the excess oxygen by oxygen annealing of the PCMO film leads to an increase of the Mn^{4+} content at the surface of the PCMO film with a subsequent change in the Mn^{4+}/Mn^{3+} ratio at the PCMO film surface. It was also reported that the oxygen content in $La_{0.75}Ca_{0.25}MnO_3$ thin films could be changed by oxygen annealing and its change resulting in cationic vacancies, and thus self-doping effect, accompanying structural changes, may be the cause of properties beyond the phase diagram.[18]

Figure 5 shows the I-V characteristics of the Au/PCMO/Pt sandwich structures in which the as-grown and the oxygen-annealed PCMO films were used to fabricate these structures. The voltage bias was scanned as $0 \rightarrow +1\ \mathrm{V} \rightarrow 0 \rightarrow -1\ \mathrm{V} \rightarrow 0$ V. Both of these structures showed the hysteretic I-V characteristics irrespective of oxygen annealing; however, they showed different resistance ratio of HRS and LRS. The magnitudes of the resistance ratio, R_H/R_L, where R_H and R_L denote resistance of HRS and LRS, respectively, were measured at ten different points of each structure at the bias voltage of +0.1 V. The mean values with the standard

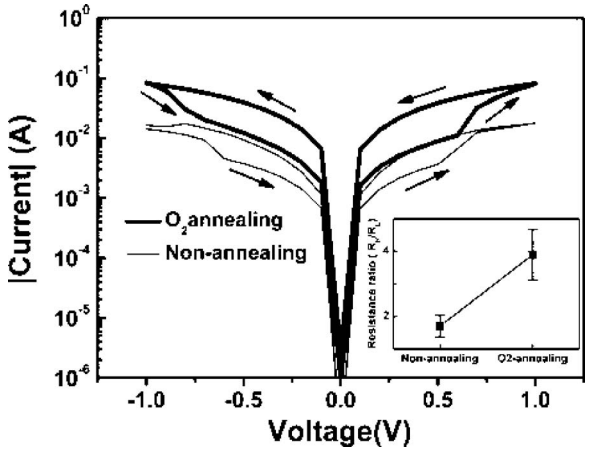

FIG. 5. I-V characteristics of Au/PCMO/Pt sandwich structures in which oxygen-annealed and as-grown PCMO films were used to fabricate these structures. Arrows indicate the direction of the sweep. The inset shows the mean values of the resistance ratio R_H/R_L with standard deviation.

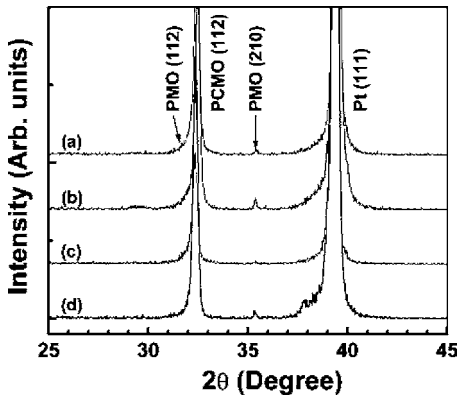

FIG. 6. XRD patterns of PMO/PCMO bilayered films deposited on $Pt/Ti/SiO_2/Si(100)$ substrates with the PMO film thickness of (a) 5 nm, (b) 10 nm, (c) 15 nm, and (d) 30 nm.

deviation are shown in the inset of Fig. 6. The resistance ratio nearly doubled by oxygen annealing of the PCMO film. This result suggests that oxygen annealing after deposition is one of the important factors to obtain the PCMO films with larger resistance ratio that is favorable to stable operation of the resistance random access memory (ReRAM) devices. Meanwhile, the oxygen-annealing dependence of the resistive switching behavior of the PCMO films may be one of important clues to elucidate the resistive switching mechanism of the PCMO films.

Figures 6 and 7 show XRD patterns of PMO/PCMO and CMO/PCMO bilayered films, respectively, which were *in situ* fabricated on $Pt/Ti/SiO_2/Si(100)$ substrates at T_s =700 °C under oxygen pressure of 300 mTorr. The thickness of the PCMO film was ~360 nm and those of PMO and CMO layers ranged from 5 to 30 nm. From these figures, it was confirmed that PMO and CMO layers grown on the PCMO films were crystallized and PMO(or CMO)/PCMO bilayered films were well-fabricated. Figures 8(a) and 8(b) show XRD patterns of PCMO(30 nm)/PMO(or CMO)(360 nm)/PCMO(30 nm) trilayered film and PMO(or CMO)(360 nm) films grown on $Pt/Ti/SiO_2/Si(100)$ substrates, respectively. These trilayered films were *in-situ* fabricated at T_s =700 °C under oxygen pressure of 300 mTorr. These figures show that these trilayered films were well prepared.

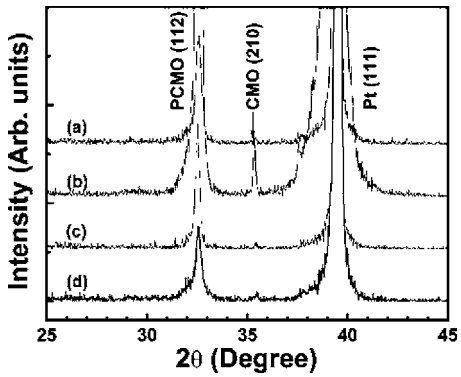

FIG. 7. XRD patterns of CMO/PCMO bilayered films deposited on $Pt/Ti/SiO_2/Si(100)$ substrates with the CMO film thickness of (a) 5 nm, (b) 10 nm, (c) 15 nm, and (d) 30 nm.

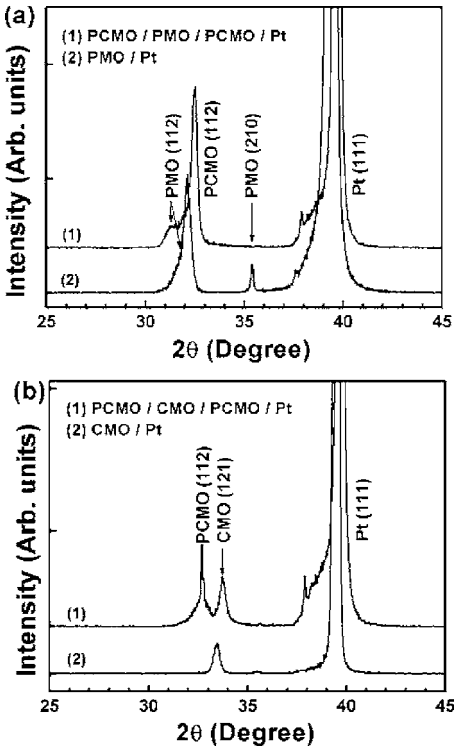

FIG. 8. XRD patterns of (a) PCMO/PMO/PCMO trilayered film and PMO film and (b) PCMO/CMO/PCMO trilayered film and CMO film deposited on $Pt/Ti/SiO_2/Si(100)$ substrates. The thicknesses of PCMO, CMO, and PMO films were 30, 360, and 360 nm, respectively.

Figure 9 shows the I-V characteristics of the Au/PMO/PCMO/Pt sandwich structure. The voltage bias was scanned as $0 \rightarrow +0.8\ V \rightarrow 0 \rightarrow -0.8\ V \rightarrow 0\ V$. This structure was found not to exhibit the hysteretic I-V characteristics irrespective of thickness of the PMO layer. It is remarkable that resistive switching did not arise by inserting thin PMO layer into Au/PCMO interface. To investigate the I-V characteristics of the PMO layer itself, Au/PMO/Pt structure was fabri-

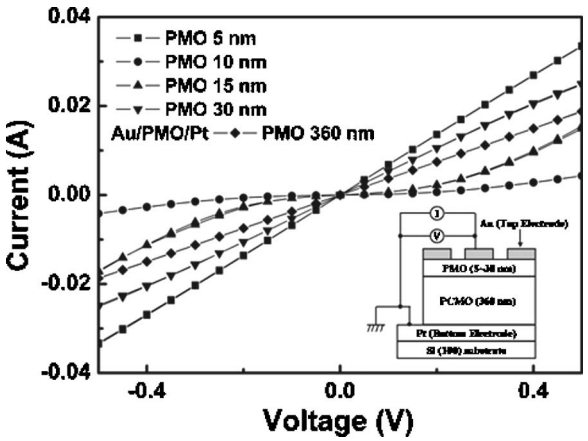

FIG. 9. I-V characteristics of Au/PMO/PCMO/Pt structures with PMO film thickness of 5–30 nm and Au/PMO/Pt structure with PMO film thickness of 360 nm. The inset shows the schematic side view of Au/PMO/PCMO/Pt structure.

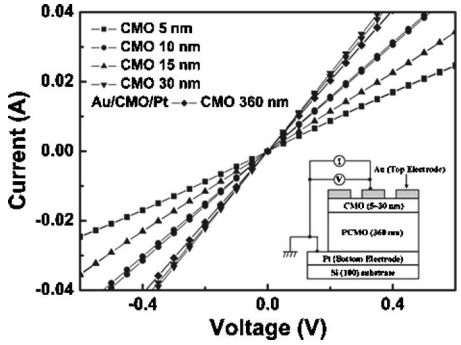

FIG. 10. I-V characteristics of Au/CMO/PCMO/Pt structure with CMO film thickness of 5–30 nm and Au/CMO/Pt structure with CMO film thickness of 360 nm. The inset shows the schematic side view of Au/CMO/PCMO/Pt structure.

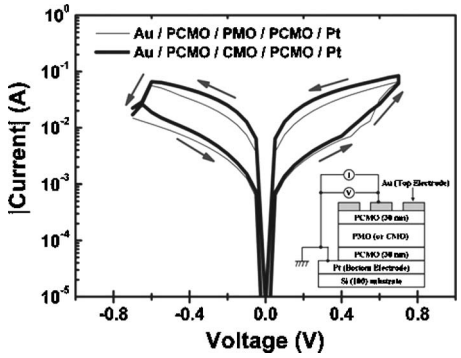

FIG. 11. I-V characteristics of Au/PCMO/PMO/PCMO/Pt and Au/PCMO/CMO/PCMO/Pt structures with arrows indicating the direction of the sweep. The inset shows the schematic side view of Au/PCMO/PMO(or CMO)/PCMO/Pt structure.

cated with the same deposition conditions for fabricating PMO/PCMO bilayered film. As a result, Au/PMO/Pt structure did not show the hysteretic I-V characteristics. As can be seen in Fig. 10, the Au/CMO/PCMO/Pt and Au/CMO/Pt sandwich structures showed almost the same I-V characteristics as those of Au/PMO/PCMO/Pt and Au/PMO/Pt ones. These results imply that the Au/PCMO interface plays a key role in the resistive switching of the Au/PCMO/Pt structure. From the viewpoint of valence state of Mn ion, these results can be explained as follows: In PCMO, Mn ions are in a mixed valence state of Mn^{4+}/Mn^{3+} resulting from coexistence of Pr and Ca ions. However, in PMO (or CMO), Mn ions are in a single valence state of Mn^{3+} (or Mn^{4+}). Therefore, it is thought that the resistive switching of the Au/PCMO/Pt structure is dependent on the mixed valence state Mn^{4+}/Mn^{3+} of Mn ions. From the result of the oxygen-annealing effect described above, it can be inferred that the Mn^{4+}/Mn^{3+} ratio is related to the resistive switching of the Au/PCMO/Pt sandwich structure: The oxygen annealing of the PCMO film increased the Mn^{4+}/Mn^{3+} ratio, resulting in an increase of the resistance ratio of HRS and LRS.

To clarify that the resistive switching of the Au/PCMO/Pt sandwich structure is dependent on the Au/PCMO interface, the Au/PCMO/PMO(or CMO)/PCMO/Pt sandwich structure was fabricated. As was expected, this structure exhibited the hysteretic I-V characteristics as shown in Fig. 11. The resistive switching occurred in the same manner as that of the Au/PCMO/Pt structure, that is, the resistive switching occurred from HRS to LRS in a positive bias region and vice versa in a negative bias region.

From the I-V characteristics of various sandwich structures, one important factor for the resistive switching phenomenon of the Au/PCMO/Pt sandwich structure was found: The PCMO films in which Mn ions are in the mixed valence state of Mn^{4+}/Mn^{3+} have to exist at both interfaces with metal electrodes. That is, in our case, Au/PCMO and PCMO/Pt interfaces have to exist for the resistive switching phenomenon, implying that the resistive switching phenomenon can be regarded as a metal/PCMO interface effect. If Mn ions are in a single valence state of Mn^{3+} or Mn^{4+} at one of both interfaces (e.g., metal/PMO or metal/CMO), the resistive switching cannot be observed.

It is notable that Rozenberg *et al.* have recently proposed a basic theoretical model for a CER effect in a metal-insulator-metal system.[13,14] The proposed model assumes several domains between the electrodes, and the current is given by the hopping of carriers from one domain to another. A large domain in the bulk behaves as a charge reservoir, and the domains at the metal/bulk interface regulate the current as barriers. Provided that the electrons in the domains near the interface are strongly correlated and exhibit the Mott transition[15] as a function of the carrier concentration, the I-V curve in the model calculation reproduces essential features of experimental results. The model predicts that the charging of the domains in the bulk is crucial for the nonvolatility of the CER behavior.[13,14,16] And also, Fors *et al.*[17] proposed that switching in the ReRAM devices is due to a shift in the valence state of a particular cation in the insulator, and that such a shift nucleates at one interface and propagates through the thickness of the insulator, creating a conduction path. This can be regarded as a Mott metal-insulator transition induced by a critical density of additional carriers added by doping. In the case of Fors *et al.*, the cation with mixed valence was Ce^{4+}/Ce^{3+} with tetravalent state representing pure insulating nonmagnetic CeO_2, and the trivalent state the paramagnetic acceptor dopants.[17] Based on these studies[13–17] for the CER model, we can present a possible scenario for the CER behavior in our case. In our case of the resistive switching of the Au/PCMO/Pt structure, metal/PCMO interface domain can regulate the currents as barriers. The metal/PCMO interface domains have the cation with a mixed valence state of Mn^{4+}/Mn^{3+} leading to exhibit a Mott metal-insulator transition induced by a critical density of additional carrier added by doping. However, in the case of Au/PMO(or CMO)/Pt and Au/PMO(or CMO)/PCMO/Pt structures, metal/PMO(or CMO) interface domain cannot regulate the current as barriers because PMO (or CMO) have the cation with a single valence state of Mn^{3+} (or Mn^{4+}). Consequently, the resistive switching of the Au/PCMO/Pt structure depends on the mixed valence state of Mn^{4+}/Mn^{3+} at the metal/PCMO interface domains.

IV. CONCLUSION

We have investigated the colossal electroresistance mechanism of the Au/PCMO/Pt sandwich structure by changing growth temperature of the PCMO films, adding an oxygen-annealing process, and modifying the Au/PCMO interface by inserting PMO or CMO layer, showing nonhysteretic I-V characteristics. From the results of these experiments, we found that the resistive switching phenomenon of this structure is strongly dependent on the mixed valence state of Mn^{4+}/Mn^{3+} at the metal/PCMO interface domains. This result can be regarded as evidence for a Mott transition and is helpful in elucidating the resistive switching mechanism of the Au/PCMO/Pt sandwich structure.

ACKNOWLEDGMENT

This research was supported by the National Research Program for the 0.1 Terabit Non-Volatile Memory Development sponsored by the Korean Ministry of Commerce, Industry, and Energy.

*Corresponding author. FAX: +82-2-958-5739. Electronic address: youngkim@kist.re.kr

[1] S. Jin, T. H. Tiefel, M. McCormack, R. A. Fastnacht, R. Ramesh, and L. H. Chen, Science **264**, 413 (1994).
[2] R. von Helmolt, J. Wecker, B. Holzapfel, L. Schultz, and K. Samwer, Phys. Rev. Lett. **71**, 2331 (1993).
[3] Y. P. Lee, J. S. Park, C. O. Kim, and V. G. Prokhorov, J. Korean Phys. Soc. **46**, S1 (2005).
[4] S. Y. Park, Y. P. Lee, and V. G. Prokhorov, J. Korean Phys. Soc. **45**, 47 (2004).
[5] V. G. Prokhorov, V. A. Komashko, V. L. Svetchnikov, Y. P. Lee, K. H. Cho, and S. Y. Park, J. Korean Phys. Soc. **45**, 22 (2004).
[6] C. Martin, A. Maignan, M. Hervieu, and B. Raveau, Phys. Rev. B **60**, 12191 (1999).
[7] S. Q. Liu, N. J. Wu, and A. Ignatiev, Appl. Phys. Lett. **76**, 2749 (2000).
[8] A. Asamitsu, Y. Tomioka, H. Kuwahara, and Y. Tokura, Nature **388**, 50 (1997).
[9] J. Sakai, A. Kitagawa, and S. Imai, J. Appl. Phys. **90**, 1410 (2001).
[10] A. Odagawa, T. Kanno, and H. Adachi, J. Appl. Phys. **99**, 016101 (2006).
[11] A. Baikalov, Y. Q. Wang, B. Shen, B. Lorenz, S. Tsui, Y. Y. Sun, Y. Y. Xue, and C. W. Chu, Appl. Phys. Lett. **83**, 957 (2003).
[12] A. Sawa, T. Fujii, M. Kawasaki, and Y. Tokura, Appl. Phys. Lett. **85**, 4073 (2004).
[13] M. J. Rozenberg, I. H. Inoue, and M. J. Sanchez, Phys. Rev. Lett. **92**, 178302 (2004).
[14] M. J. Rozenberg, I. H. Inoue, and M. J. Sanchez, Appl. Phys. Lett. **88**, 033510 (2006).
[15] M. Imada, A. Fujimori, and Y. Tokura, Rev. Mod. Phys. **70**, 1039 (1998).
[16] A. Odagawa, H. Sato, I. H. Inoue, H. Akoh, M. Kawasaki, Y. Tokura, T. Kanno, and H. Adachi, Phys. Rev. B **70**, 224403 (2004).
[17] R. Fors, S. I. Khartsev, and A. M. Grishin, Phys. Rev. B **71**, 045305 (2005).
[18] W. Prellier, M. Rajeswari, T. Venkatesan, and R. L. Greene, Appl. Phys. Lett. **75**, 1446 (1999).
[19] B. Dabrowski, P. W. Klamut, Z. Bukowski, R. Dybzinski, and J. E. Siewenie, J. Solid State Chem. **144**, 461 (1999).